The Hepatitis Delta Antigen Retains the Assembly Domain as the Only Rigid Entity

Yang Yang, Marie-Laure Fogeron, Alexander A Malär, Lauriane Lecoq, Alexander B Barnes, Beat H Meier, Anja Böckmann, Morgane Callon

The Hepatitis Delta Antigen Retains the Assembly Domain as the Only Rigid Entity

Yang Yang[1], Marie-Laure Fogeron[1], Alexander A. Malär[2], Lauriane Lecoq[1], Alexander B. Barnes[2], Beat H. Meier[2], Anja Böckmann*[1], Morgane Callon*[1]

[1] Molecular Microbiology and Structural Biochemistry (MMSB) UMR 5086 CNRS/Université de Lyon, Labex Ecofect, 7 passage du Vercors, 69367 Lyon, France

[2] Department of Chemistry and Applied Biosciences, ETH Zurich, 8093 Zurich, Switzerland

* Corresponding authors: a.bockmann@ibcp.fr, morgane.callon@ibcp.fr

Keywords: Hepatitis Delta virus, small antigen, ^{1}H-MAS NMR, resonance assignments

Abstract

The hepatitis delta virus (HDV) S-HDAg and L-HDAg antigens are the two isoforms of the single protein encoded by the viral genome. Together with the double-stranded RNA genome they form the HDV ribonucleoprotein (RNP) complex. In the context of a divide-and-conquer approach, we used a combination of cell-free protein synthesis (CFPS) and proton (^{1}H)-detected fast magic angle spinning (MAS) solid-state NMR at highest magnetic field to characterize S-HDAg. We sequentially assigned *de-novo* its isolated N-terminal assembly domain using less than 1 mg of fully protonated protein. Our results show that the assembly domain is the sole rigid component in S-HDAg, with its structure remaining fully conserved within the full-length protein. In contrast, the rest of the protein remains dynamic. This work provides the necessary foundation for future studies of the viral RNP.

Introduction

Hepatitis D (or delta) is an inflammatory disease of the liver caused by the hepatitis delta virus (HDV), which relies on the hepatitis B virus (HBV) for replication, since the latter provides the envelope proteins for viral particle formation in the context of co-infection[1]. HBV has a worldwide distribution, with nearly 5% of people with chronic HBV infection also infected with HDV. This often leads to a more aggressive form of hepatitis, with rapid progression to liver cirrhosis and an increased risk of hepatocellular carcinoma[2]. HDV carries a 1700-base circular RNA genome, that is mostly double-stranded, resulting in the formation of a rod-like structure[3]. The hepatitis delta antigen (HDAg) is the only protein encoded by the genome. It exists in two isoforms, the small and the large delta antigens (S-HDAg and L-HDAg respectively). S-HDAg, which is 195 amino acids long, is essential for HDV replication[4,5]. L-HDAg has a C-terminal addition of 19 amino acids, resulting in a 214 amino acid form[6]. S-HDAg is required for HDV genome replication[5], while L-HDAg hinders this process[7,8]. L-HDAg is essential for ribonucleoprotein (RNP) packaging by the HBV envelope proteins[9,10].
The N-terminal assembly domain of HDAg, from residues 12 to 60, was identified early on and its structure was solved by X-ray crystallography using a synthetic peptide[11]. Each monomer consists of a long helix interrupted by a turn, and another short helix. The protein forms a dimer in which the long helices gather into an antiparallel coiled coil structure. In the crystal, it further assembles into octamers[11], which can also form during HDV replication[12]. The capacity of the protein to form multimers and its ability to bind specifically to HDV RNA[13,14] suggest its involvement in the formation of the RNP[15], yet the molecular details of this process remain to be determined. While predictions were available previously[16], we have recently experimentally determined the 3D structure of the C-terminal domain of S-HDAg (S-HDAg$^{\Delta 60}$), from residues 61-195, using solution-state NMR (Yang et al., submitted), and established the RNA-binding properties of this domain. However, structural studies of the full-length S-HDAg protein remain unavailable at the present time, probably due to its high aggregation propensity[17].

Here, we address the S-HDAg protein, and in a divide-and-conquer approach also its isolated assembly domain, HDAg$^{1\text{-}60}$. The use of cell-free protein synthesis (CFPS)[18,19] represents a significant advantage in this strategy, as it produces the protein aggregates as the sole isotope-labeled component of the reaction. This largely eliminates the need for further processing, although pellet washing after CFPS improves the purity of the recovered protein assembly. One can mention that for soluble proteins, we remove impurities using single-step affinity purification[20–22]. The preparation is then directly analyzed by high-field proton-detected magic-angle-spinning NMR (^{1}H-MAS-NMR), compatible with the sub-milligram amounts

obtained[20,21,23–25]. The NMR fingerprints identify HDAg$^{1-60}$ as the only rigid part of HDAg, and resonance assignments of its fully protonated form show that the structure of the assembly domain is largely conserved within S-HDAg, thereby elucidating its structural organization.

Results

NMR sample preparation of S-HDAg and HDAg$^{1-60}$ assembly domain

We produced the S-HDAg protein and its isolated assembly domain HDAg$^{1-60}$ (Fig. S1a) using wheat germ (WG) CFPS[18], as summarized in Fig. 1a. Following the addition of the mRNA encoding the protein to the cell-free reaction, the protein of interest is synthesized overnight. It is then isolated by centrifugation where it separates into the pellet (i.e. insoluble) fraction, confirming its previously observed high aggregation propensity[17]. Consequently, the protein could not be purified without perturbing its native state, and we used a simple washing step to remove some of the unlabeled contaminants from the newly synthesized and thus isotopically labeled protein. The resuspended pellet (P in Fig. 1b,c and Fig. S2) is then centrifuged directly into the MAS rotor. The entire sample preparation process takes less than 2 days. The protein yield for both S-HDAg and HDAg$^{1-60}$ is approximately 1 mg per ml of WG extract (WGE) used, sufficient to fill a 0.7 mm MAS rotor. We have used the same approach to produce selectively labeled samples, where the added amino acids reflect the desired labeling scheme.

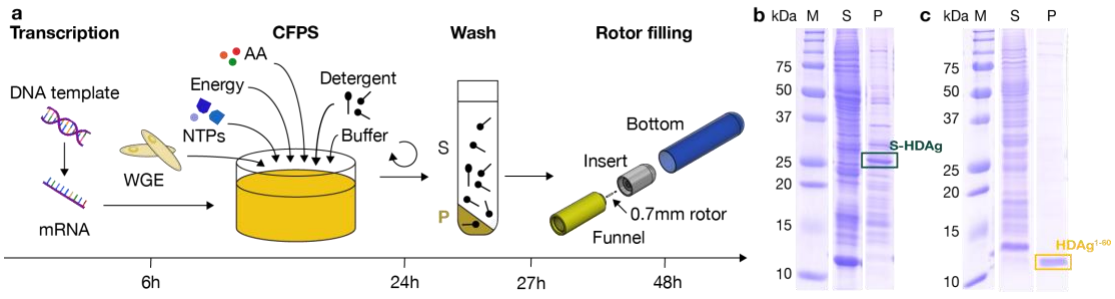

Figure 1. NMR sample preparation. **a)** mRNA template is translated into the protein in the CFPS reaction (see Materials and Methods for details). The washed and resuspended pellet is sedimented into a 0.7 mm NMR rotor using a home-made filling tool[26]. Coomassie stained gels of **b)** CFPS of [^{2}H,^{13}C,^{15}N]-labeled (DUL) S-HDAg and **c)** of DUL-HDAg$^{1-60}$. The supernatant (S) and pellet (P) fraction of the total cell-free reaction are shown.

The assembly domain is conserved in S-HDAg, and represents its only rigid part

We first recorded a 2D hNH fingerprint NMR spectrum of [^{2}H,^{13}C,^{15}N]-labeled (DUL) S-HDAg (Fig. 2a,b). One can note that since CFPS is carried out in H_2O, all labile protons are protonated. The chemical shift dispersion of the amide protons (H_N), ranging from 6.3 ppm to 9.5 ppm, is indicative of a folded protein (full spectrum in Fig. S3). The spectrum shows well resolved resonances, but their number is significantly lower than the expected 195. To identify the resonances observed in the S-HDAg spectrum, we then prepared a sample of DUL HDAg$^{1-60}$ (Fig. 2a). A comparison of the 2D hNH spectra of the two proteins in Fig. 2c reveals that they share a similar set of resonances, suggesting that the peaks of S-HDAg originate from the HDAg$^{1-60}$ domain. Since the cross-polarization-based (CP) based hNH NMR spectra reveal only rigid parts, we conclude that the remaining residues of S-HDAg (61 to 195) must be dynamic. Both spectra show about 40 resolved resonances, meaning that also only parts of HDAg$^{1-60}$ are visible. A comparison of the S-HDAg and HDAg$^{1-60}$ 1D hnH spectra reveals a significant difference in signal-to-noise ratio (SNR) (Fig. 2f, green and yellow spectra, respectively). This is due to the three times larger protein, and the fact that the S-HDAg sample contains more contaminants (Fig. 1b,c).

The NMR resonance linewidth is an indicator of sample homogeneity. We therefore measured the total amide proton linewidth ($\Delta^{tot}(H_N)$) for a selection of 14 isolated peaks (Table S1), as shown for two selected resonances in Fig. 2g. The median values are shown in Fig. 2h (bar plot in Fig. S4), and reveal that DUL-S-HDAg and DUL-HDAg$^{1-60}$ have similar linewidths of about 0.14 ppm, comparable to the average linewidths measured for the HBV capsid at a similar MAS frequency[25].

We also prepared a [^{13}C,^{15}N] uniformly labeled (UL) HDAg$^{1-60}$ sample for side-chain assignments, whose 2D hNH spectrum is compared with DUL-HDAg$^{1-60}$ in Fig. 2d. The linewidths are on average about 40% broader due to the denser proton dipolar-coupling network. The use of high magnetic field (1.2 GHz proton frequency) allowed to reduce the linewidth, including the homogeneous contribution (Table S2), below that of DUL HDAg$^{1-60}$ (in red in Fig. 2 and Figs. S3,4), and significantly improved resolution in the 2D hNH (Fig. 2e), as previously observed for other proteins[27]. We therefore recorded further 3D spectra for sequential assignments at 1.2 GHz.

Taken together, our data show that the structure of the oligomerization domain appears to be largely conserved in S-HDAg, and represents its only rigid part, since the C- terminal S-HDAg$^{\Delta 60}$ domain remains dynamic.

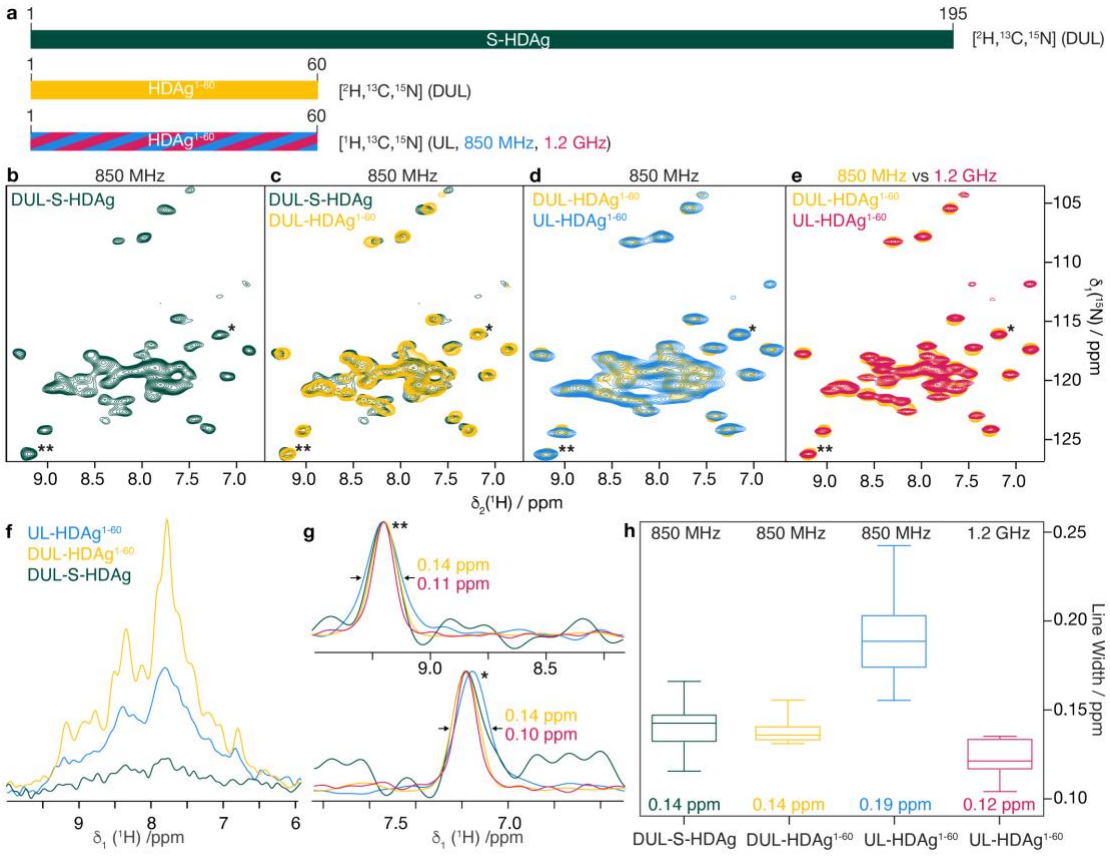

Figure 2. **The assembly domain is observed in the hNH spectra of S-HDAg. a)** Schematic representation of the different protein constructs analyzed and their labeling**. b)** 2D hNH spectrum of DUL-S-HDAg (dark green) and **c)** overlay with DUL-HDAg$^{1-60}$ (yellow). **d)** Overlay of the 2D hNH spectra of DUL-HDAg$^{1-60}$ (yellow) with UL-HDAg$^{1-60}$ (blue). The spectra in panels b-d are recorded at 100 kHz MAS frequency and 850 MHz proton Larmor frequency. **e)** Overlay of the 2D hNH spectra of DUL-HDAg$^{1-60}$ (yellow) and UL-HDAg$^{1-60}$ (magenta) recorded at 100 kHz MAS frequency and at 850 MHz and 1.2 GHz proton Larmor frequencies respectively. **f)** Overlay of the first FIDs of the 2D hNH spectra of DUL-S-HDAg (dark green), DUL-HDAg$^{1-60}$ (yellow) and UL-HDAg$^{1-60}$ (blue) shown in panels a to c. **g)** 1D ^{1}H traces for resonances labeled with * and ** (δ_1 (^{15}N) = 116.19 and 126.33 ppm respectively) from the 2D hNH spectra in panels b-e. $\Delta^{tot}(H_N)$ is given for DUL HDAg$^{1-60}$ (yellow) and UL HDAg$^{1-60}$ (red). **h)** Box plots of $\Delta^{tot}(^{1}H_N)$ (Table S1 and Fig. S4) of 14 selected isolated peaks in the 2D hNH spectra shown in Fig. 2b-e. The median total proton linewidth is given.

Sequential backbone resonance assignments of HDAg$^{1-60}$

In order to compare S-HDAg and HDAg$^{1-60}$ in more detail, we sequentially assigned the resonances of the latter using 3D hCANH, hCAcoNH, hNCAH, hNcoCAH and hCONH experiments[28] recorded on UL HDAg$^{1-60}$. Inter- and intra-residue correlations are shown in Fig. 3a,b at the example of residues W20, V21 and A22. Transfer efficiencies of the different experiments are given in Fig. S5.

These spectra allowed for the *de-novo* assignment of 28 residues of HDAg$^{1-60}$. Peak overlap, especially in the regions of the multiple Lys and Glu residues, prevented further assignments. We thus produced two selectively labeled samples, EL-HDAg$^{1-60}$ and GRK-HDAg$^{1-60}$, which 2D hNH spectra are shown in cyan and orange in Fig. 3c respectively. The sequential assignment of the labeled amino acids was supported by peaks in the hCONH (Fig. 3d) and hCAcoNH (Fig. S6) spectra, showing exclusively pairs of labeled amino acids. In the hCONH we observed 5 out of 6 expected resonance pairs for EL-HDAg$^{1-60}$, and 6 out of 9 for GRK-HDAg$^{1-60}$ (Fig. 3d). 4 out of 6 and 5 out of 9 pairs could be detected in the 3D hCAcoNH, where the SNR suffers from the additional $^{13}C\alpha$-$^{13}C'$ transfer (Fig S5). The selectively labeled samples allowed for the assignment of 11 additional amino acids. It should be noted that although scrambling is limited in WGE[29], for EL-HDAg$^{1-60}$ one weak Ala and two Asp signals were observed in the 2D hNH (Fig. 3c), and one weak Asp and one Gln signals in the 2D hCH spectra (Fig. S7). No scrambling was observed for GRK-HDAg$^{1-60}$.

Residues 1-13 were not detected in any of the spectra, suggesting that the very N-terminal region is dynamic. Residues 1-11 were not present in the previous X-ray study[11]. In addition to the undetected N-terminal residues, we could not detect K60, probably due to its proximity to the flexible tag. Strong overlap prevented assignment of K40-K43 and R32/R35. In total, we assigned the backbone resonances of 83% of the visible residues in HDAg$^{1-60}$.

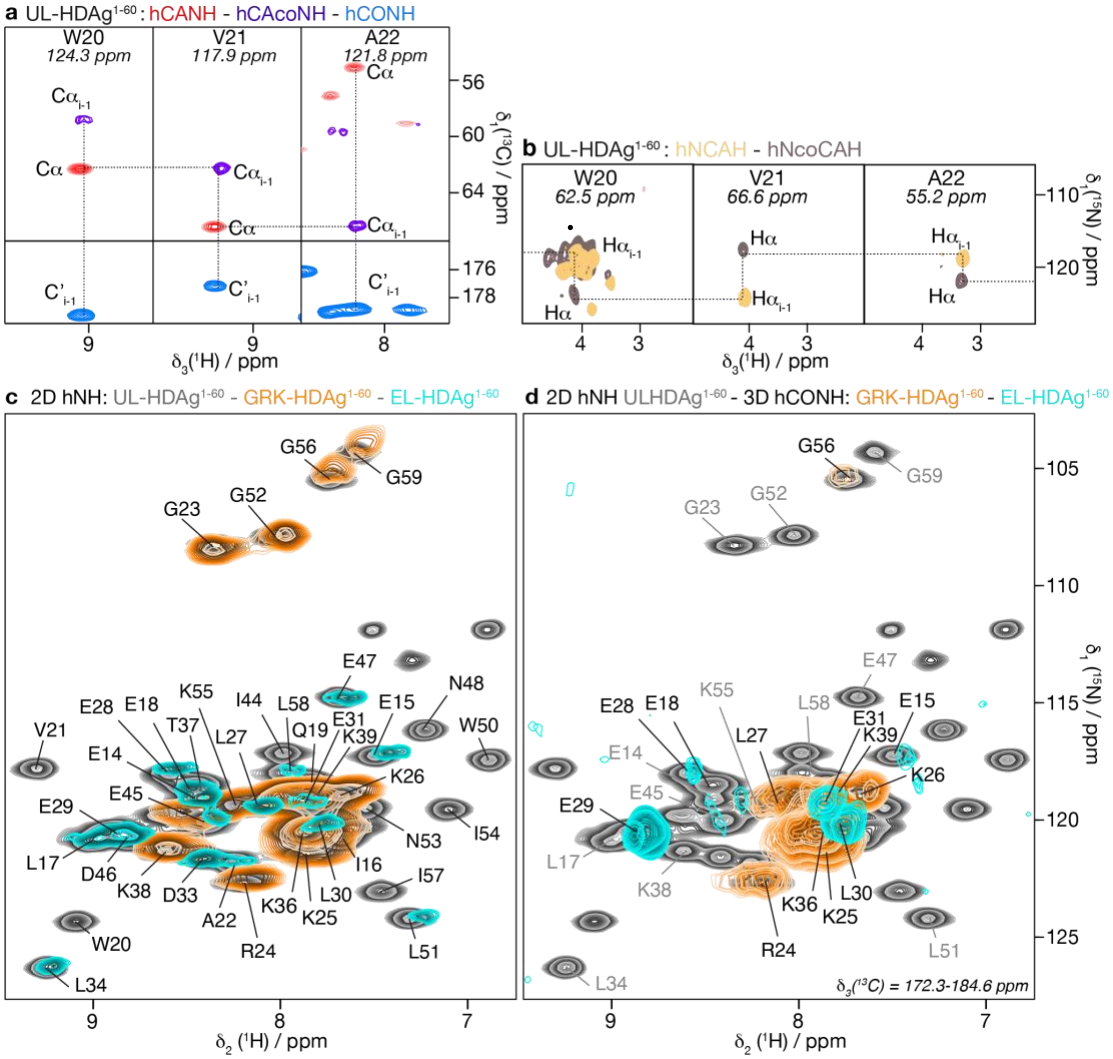

Figure 3. **HDAg$^{1-60}$ backbone resonance assignment. a)** 2D strips extracted from 3D hCANH (red), hCAcoNH (purple) and hCONH (blue) spectra of UL-HDAg$^{1-60}$ for resonances W20-A22. Connections are obtained by matching the Cα frequencies. **b)** 2D strips extracted from 3D hNCAH (yellow) and hNcoCAH (light brown) spectra of UL-HDAg$^{1-60}$ for resonances W20-A22. Connections are obtained by matching the N frequencies. **c**) Overlay of the 2D hNH spectrum of UL-HDAg$^{1-60}$ (grey) with 2D hNH spectra of EL-HDAg$^{1-60}$ (cyan) and GRK-HDAg$^{1-60}$ (orange) and **d)** with 3D- hCONH spectra of EL-HDAg$^{1-60}$ (cyan) and GRK-HDAg$^{1-60}$ (orange). All spectra are recorded at 100 kHz MAS and 1.2 GHz (except the 3D hCONH spectrum of EL-HDAg$^{1-60}$ recorded at 850 MHz). The resonances marked in grey are not visible in the 3D hCONH spectra because their preceding amino acid is not [^{13}C,^{15}N]-labeled.

Side chain resonance assignment of HDAg$^{1-60}$

We first recorded a 2D hCH spectrum for which extracts are given in Fig. 4a (full spectrum in Fig. S7). The Hα-Cα region shows the expected chemical shift dispersion, and the median total H_α linewidth $\Delta^{tot}(H_\alpha)$ is 0.17 ppm, based on a selection of 14 isolated peaks. This corresponds to 200 Hz on a 1.2 GHz magnet, (Table S3), which is higher than for the amide protons (146

Hz). This is consistent with the shorter $T_2'(H_{ali})$ of 2.1 ms we measured for the aliphatic protons compared to $T_2'(H_N)$ = 2.5 ms for the amide protons (Table S2), revealing the stronger dipolar coupling network and smaller chemical shift difference they experience with neighboring proton spins[27].

Starting from the Cα/Hα resonances, we assigned the ^{13}C and ^{1}H side chain resonances by using a 3D hCCH TOBSY spectrum[30] recorded on the UL and GRK labeled samples (Fig. 4b). Correlations for residue K36 are shown as an example in Fig. 4b on the GRK-$HDAg^{1-60}$ hCCH. Despite the small size of the protein, the modest dispersion due to the fully α-helical structure and the multiple Leu, Lys and Arg residues resulted in some spectral overlap, as seen in the 2D hCH extracts in Fig. 4c,d (full spectra in Fig. S7). Nevertheless, the two protons of many CH_2 groups showed resolved peaks (Fig. 4e).

In total we assigned 38% of the proton and 36% of the non-proton side-chain resonances for the visible residues of $HDAg^{1-60}$. The assignment of 63% of the Cβ resonances, but only 33% of the Cδ resonances (see Table S4 for details) reflects the poorer dispersion of the resonances from spins further away from the backbone.

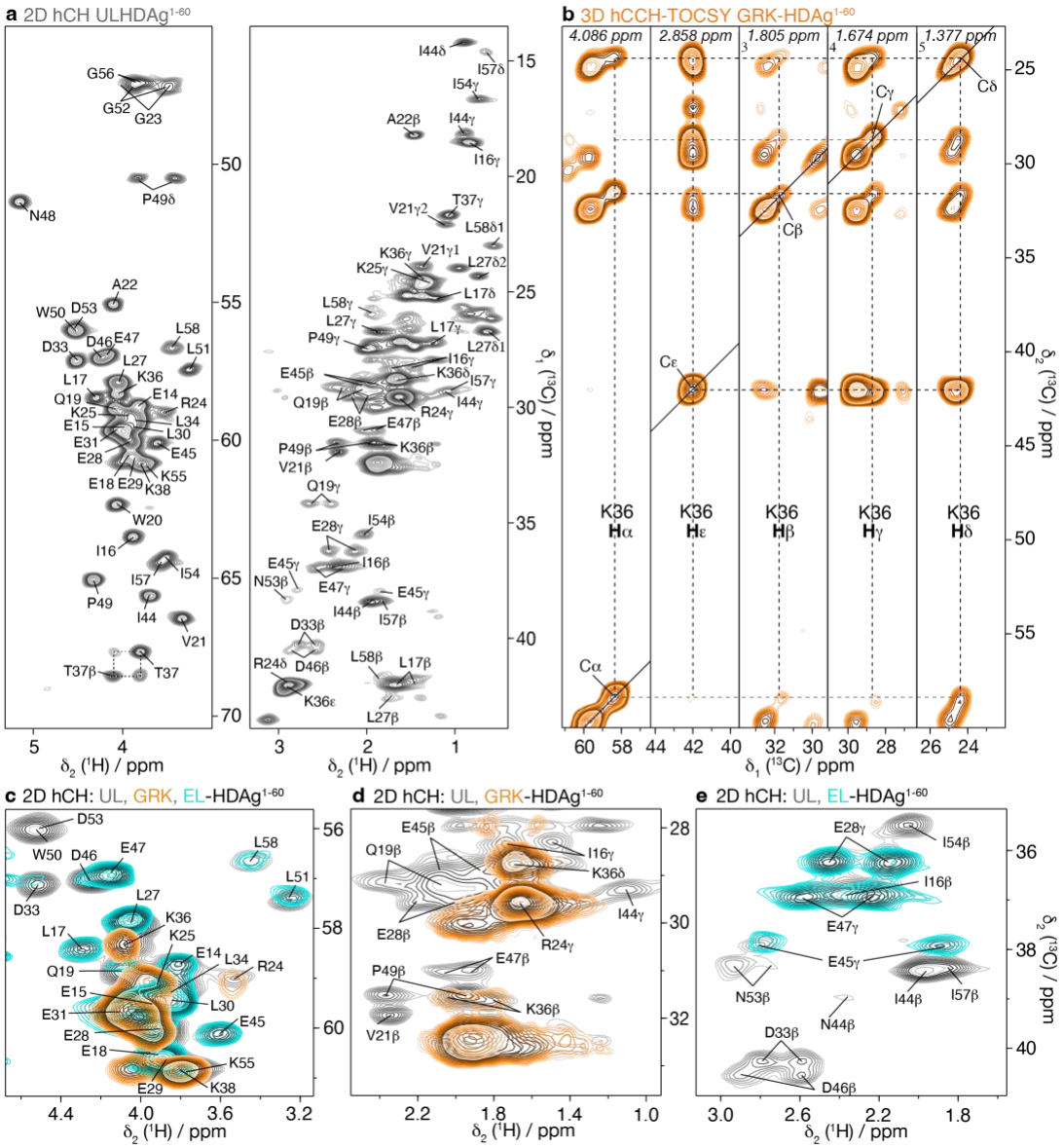

Figure 4. **HDAg$^{1-60}$ side-chain resonance assignment**. **a)** Hα-Cα (left) and side-chain (right) regions of the 2D hCH spectrum of UL-HDAg$^{1-60}$ (grey) recorded at 100 kHz MAS and 1.2 GHz. **b)** CC strips of the hCCH-TOCSY spectra of GRK-HDAg$^{1-60}$ for residue K36. The ^{1}H chemical shifts of the resonances are indicated in italic. **c)** Extract of the Hα-Cα region of the 2D hCH spectra of UL-HDAg$^{1-60}$ (grey), EL-HDAg$^{1-60}$ (cyan) and GRK-HDAg$^{1-60}$ (orange). **d)** Extract of the side chain region of the 2D hCH spectra of UL-HDAg$^{1-60}$ (grey) and GRK-HDAg$^{1-60}$ (orange). **e)** Extract of the side chain region of the 2D hCH spectra of UL-HDAg$^{1-60}$ (grey) and EL-HDAg$^{1-60}$ (cyan).

Summary of resonance assignments and derivation of secondary chemical shifts

This *de novo* ^{1}H-MAS NMR assignment of a fully protonated protein was done without prior knowledge of solid- or solution-state NMR chemical shifts. We provide here a brief overview of the spectrometer time required and the resulting completeness. Spectra for the UL-HDAg$^{1-60}$ backbone assignments were acquired in 11 days, and for the selectively labeled samples in

12 days. Experiments for side chain assignments took 5 days. We obtained at least partial assignments for 91% of the residues. We achieved a backbone (H^N, N, Hα, Cα and C') assignment completeness of 83% for residues visible in $HDAg^{1-60}$ (14-60), and a side chain assignment completeness of 37% (Table S4). Higher completeness could be achieved by using additional selective labeling schemes or a combinatorial approach[31]. As sample preparation is fast, the NMR measurement time remains the limiting step. Further development of dedicated solid-state NMR combinatorial labeling approaches[31–34] will be a future asset.

Obtained assignments immediately identify secondary structure elements via secondary chemical shifts (ΔδCα-ΔδCβ)[35]. We calculated them and compared them to the previously determined $HDAg^{12-60}$ X-Ray structure[11] (Fig. 5a). This validates the assignments and confirms the presence in the structure (Fig. 5b, PDB 1a92[11]) of two helices interrupted by a sharp bend at residue N48. Even if we do not report any distance constraints, the fact that the resonances of 51L, which is sandwiched in the X-ray structure[11] between two Trp residues (W20/W50) from different monomers (Fig. S8), are strongly shielded indicates that the presence of the corresponding structural element in the NMR sample is highly likely. This demonstrates how chemical shifts can in certain cases also verify the higher-dimensional arrangement of molecular structures.

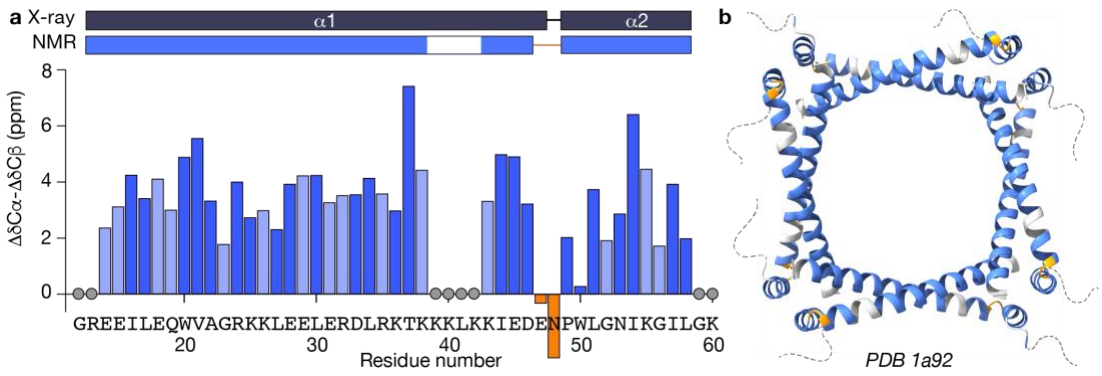

Figure 5. **Secondary structure prediction from chemical shifts**. **a)** Secondary chemical shifts[36] of UL-$HDAg^{1-60}$ as a function of residue number. Light blue bars indicate secondary chemical shifts for which only the Cα chemical shift was considered because the residue is a glycine or because the Cβ could not be assigned. Orange bars indicate negative values. Grey circles represent unassigned residues. Secondary structure elements observed in the X-ray structure (PDB 1a92)[11] are shown in dark blue at the top. **b)** The NMR-derived secondary structure is mapped in blue on the X-ray structure (PDB 1a92)[11], with residues E47 and N48 shown in orange. Unassigned residues are shown in light grey.

The assembly domain is conserved in the full-length protein

The similarity of the S-HDAg to the HDAg$^{1-60}$ spectra (Fig. 2c) allowed us to transfer most of the assignments (Fig. S9). We measured the chemical shift differences between HDAg$^{1-60}$ and S-HDAg for the isolated resonances in the 2D hNH spectra, shown in Fig. 6a for H_N and N respectively. While they remain generally small, significant differences are observed for some residues (in red in Fig. 6a), which are mainly localized at the interdimer interface around residues 15-28 as shown in Fig. 6b on the octamer structure[11]. We have observed that the presence of the Strep tag at the HDAg$^{1-60}$ C-terminus also affects some of these residues (Fig. S10), albeit resulting in different chemical shifts. This makes it likely that the residues attached to HDAg$^{1-60}$, whether from the tag or from S-HDAg, have some interaction with the residues beyond 60. No differences are observed in the middle of the coiled coil domain.

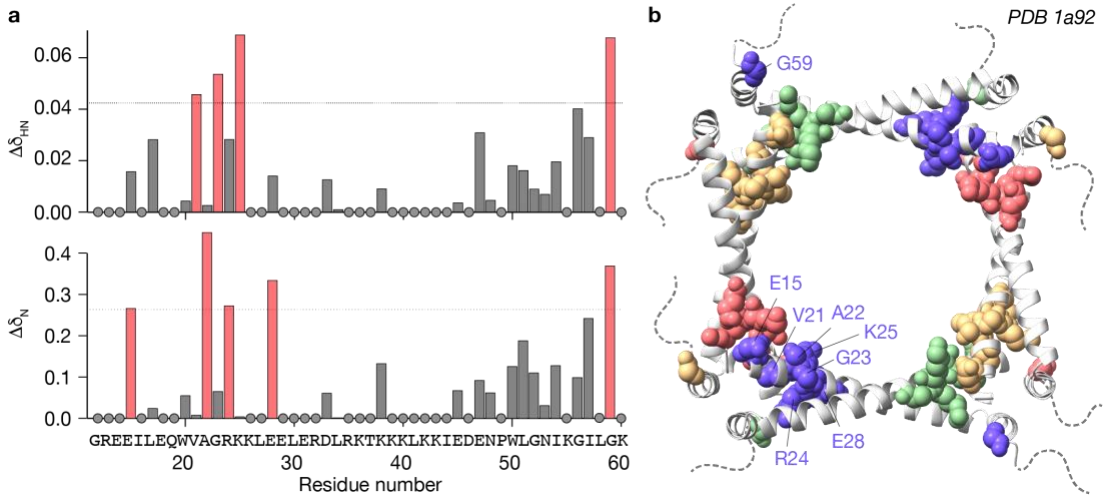

Figure 6. Chemical shift differences observed between S-HDAg and HDAg$^{1-60}$. a) Differences in amide proton chemical shift ($\Delta\delta_{HN}$) and in nitrogen chemical shift ($\Delta\delta_N$) observed between S-HDAg and HDAg$^{1-60}$ for 23 isolated resonances in the 2D hNH spectra (Fig 2c). The unassigned/unresolved residues are shown as grey circles. The threshold value is shown as a dotted line and corresponds to one standard deviation above the mean chemical shift difference **b)** Residues with significant $\Delta\delta_{HN}$ or $\Delta\delta_N$ (red bars in panel a) are colored on the octameric structure and represented as spheres (PDB 1a92)[11]. The monomers are shown in different colors.

Discussion and conclusion

We here studied the conformation of S-HDAg, for which no structural information was previously available. We have successfully used CFPS to produce the protein for NMR

structural studies, despite its tendency to form insoluble aggregates. We have shown that the structure of the $HDAg^{1-60}$ assembly domain is largely conserved within the full-length S-HDAg protein and that residues 14-60 represent the only rigid part of the protein. NMR spectra of S-HDAg show that the S-$HDAg^{\Delta 60}$ domain, which is soluble in isolation[16], remains flexible within the full-length protein. Our data also suggest that the dimeric form identified for $HDAg^{12-60}$ is likely present in the NMR sample.

Our study demonstrates the feasibility to directly investigate the aggregated forms of proteins present in the pellet fraction of the CFPS reaction after centrifugation. While we have reported a similar observation for the regular capsid assemblies formed by the HBV core protein[37], the HDAg aggregates do not form any regular structures observable under the microscope. However, the resolution of the NMR signals is similar, indicating that the proteins form homogeneous assemblies on shorter length scales. Impurities from the CFPS reaction mixture do not affect the quality of the spectra, but affect the signal/noise if present in excess. While the low signal-to-noise ratio (SNR) observed for S-HDAg made sequential assignments difficult, the similarity of the chemical shifts showed that $HDAg^{1-60}$ can be used as a proxy for the full-length protein for assignments. The only small differences observed between the isolated domain and the domain in the context of the full-length protein confirmed the validity of the divide-and-conquer approach. These differences localized to the interdimer interaction sites, suggesting that the superstructural assembly may be slightly modified by the presence of the C-terminal portion of the protein.

The use of the highest available magnetic field, combined with fast MAS and selective labeling, provided sufficient resolution of this fully labeled protein, especially for the side chains, allowing the assignment of substantial portions of this small, but poorly dispersed, exclusively α-helical protein. These assignments are among the first ones obtained without prior chemical shift knowledge, solely using ^{1}H-MAS NMR on a fully protonated protein. They thus demonstrate the potential of this approach for studies where small amounts of protein are available, and the use of larger NMR rotors is not an option. Our work highlights that deuteration is not necessary to obtain backbone assignments, which also avoids chemical shift corrections[38] when performing side-chain assignments on protonated samples.

Our work represents an important step toward the residue-specific characterization of the HDV ribonucleoprotein complex. While we have demonstrated that the C-terminal domain of S-HDAg binds to *in vitro* synthesized viral RNA (Yang et al. submitted), the RNA binding properties of the assembly domain remain undescribed. The current understanding, namely that the assembly domain may form a nucleosome-like particle in which the double-stranded RNA wraps around multiple octameric assemblies[17,39–41], lacks an experimental basis today. The current work paves the way for further investigations of the RNP.

Materials and Methods

Plasmids

The cDNA encoding the full-length S-HDAg (HDV genotype 1 Central African AJ000558.1, Fig. S1a), and $HDAg^{1\text{-}60}$ (Fig. S1b) were cloned into the pEU-E01-MCS vector (CellFree Sciences, Japan). The resulting plasmids were amplified into *Escherichia coli* TOP10 competent cells (Life Technologies). DNA extraction was performed using the NucleoBond Xtra Maxi kit (Macherey-Nagel, France). Plasmids were further purified by phenol/chloroform extraction according to the recommendations of CellFree Sciences (Yokohama, Japan).

Wheat germ cell-free protein synthesis of S-HDAg and $HDAg^{1\text{-}60}$

The proteins were synthesized using WG-CFPS following protocols outlined in Takai et al.[18] and Fogeron et al.[42]. Home-made WG extract was prepared using non-treated durum wheat seeds (Florimond-Desprez, France) as described in[18,42]. Cell-free protein synthesis was performed using uncoupled transcription and translation. Transcription was performed using 100 ng/µl plasmid, 2.5 mM NTP mix (Promega, France), 1U/µl RNase inhibitor (CellFree Sciences, Japan) and 1U/µl SP6 RNA polymerase (CellFree Sciences, Japan) in the transcription buffer containing 80 mM Hepes-KOH pH 7.6, 16 mM magnesium acetate, 10 mM DTT and 2 mM spermidine (CellFree Sciences, Japan) (listed in Table S5). The solution was incubated for 6 h at 37 °C, and the mRNA produced was used directly for translation. Translation was performed using either the bilayer method for the different $HDAg^{1\text{-}60}$ samples (see below) or using the dialysis mode for the [^{2}H,^{13}C,^{15}N]-labeled S-HDAg sample. For selectively labeled samples, [^{13}C,^{15}N] Gly, Arg and Lys or Glu and Leu amino acids (Cambridge Isotope Laboratories) were used. For uniformly [^{2}H,^{13}C,^{15}N] and [^{13}C,^{15}N] labeled

samples, [^{2}H,^{13}C,^{15}N] and [^{13}C,^{15}N] cell-free amino-acid mix (20 aa) (Cambridge Isotope Laboratories CDNLM-6784 and CNML-6696), were used respectively.

HDAg$^{1-60}$ translation was carried out in the bilayer mode in 6-well plates. The bottom layer corresponding to the translation mixture contained per well ½ volume of mRNA, ½ volume of WGE, 40 ng/ml creatine kinase and 6 mM of amino acid mix and 0.1% MNG-3 detergent. The upper layer, corresponding to the feeding buffer, contained SUB-AMIX NA (CellFree Sciences; 30 mM Hepes-KOH pH 7.6, 1.2 mM ATP, 0.25 mM GTP, 16 mM creatine phosphate, 0.4 mM spermidine, 2.7 mM magnesium acetate and 100 mM potassium acetate, 4 mM dithiothreitol), supplemented with 6 mM amino acid mix and 0.1% MNG-3 detergent (listed in Table S6) The translation reaction was incubated for 20 h at 22 °C without agitation.

Translation of S-HDAg was carried out in the dialysis mode in a 3-ml dialysis cassette with a MWCO of 10 kDa. The translation mixture inside the cassette contained ½ volume of feeding buffer, 1/3 volume of mRNA, 1/6 volume of WGE, 40 ng/µL of creatine kinase, 6 mM of amino acid mix, and 0.05% Brij-58. The feeding buffer in which the cassette was immersed contained SUB-AMIX NA (CellFree Sciences), supplemented with 6 mM of amino acid mix, and 0.05% Brij-58 (listed in Table S6). The translation reaction using this mode was run for 20 h, at 22°C and 70 rpm. It should be noted that the bilayer mode, while providing similar yields per ml of WGE used, requires addition of fewer amino-acids but results in lower protein concentrations due to mixing with the feeding buffer. The total cell-free samples (CFS) were treated with benzonase for 40 min at room temperature.

NMR sample preparation

After addition of 20 µl of saturated 4,4-dimethyl-4-silapentane-1-sulfonic acid (DSS) solution, the total CFS of the [^{2}H,^{13}C,^{15}N]-S-HDAg sample was directly sedimented into a 0.7 mm MAS NMR rotor by ultracentrifugation (14 h, 200,000g, 4°C) using home-made filling tools[43].

Four samples of HDAg$^{1-60}$ were prepared, with different labeling schemes: (1) [^{2}H,^{13}C,^{15}N]-labeled (DUL-HDAg$^{1-60}$), with labile protons being protonated; (2) [^{13}C,^{15}N]-labeled (UL-HDAg$^{1-60}$), (3) [^{13}C,^{15}N] Glu and Leu labeled, with other amino acids deuterated (EL-HDAg$^{1-60}$) and (4) [^{13}C,^{15}N]-Gly, Arg and Lys labeled, with other amino acids deuterated (GRK-HDAg$^{1-60}$). In addition, a UL-HDAg$^{1-60}$ sample without strep tag was prepared. The total CFS HDAg$^{1-60}$ was centrifuged at 4 °C, 200,000 g for 1 hour using a JA-20 fixed angle rotor (Beckman Coulter) to obtain a pellet. To remove higher molecular weight impurities, the sediment was resuspended in 0.1 % DDM for 1h, followed by centrifugation for 30 min at 4 °C, 200,000 g. The pellet was resuspended in 400 µl of wash buffer (100 mM Tris-Cl, 150 mM NaCl, 1 mM EDTA, pH 8) 1x and 20 µl of saturated DSS solution was added to the protein for

chemical shift referencing prior to the sedimentation into a 0.7 mm MAS NMR rotor by centrifugation (14 h, 200,000g, 4°C) using home-made filling tools[43].

NMR spectroscopy

The solid-state NMR experiments were recorded at static magnetic field strengths of 20.0 and 28.2 T (wide-bore 850 MHz Bruker Avance III and standard-bore 1.2 GHz Bruker Avance NEO spectrometers, respectively). All experiments were recorded at a MAS frequency of 100 kHz in a 0.7 mm triple-resonance probe head (Bruker Biospin). Sample temperatures between 20 and 25°C were estimated from the relationship T(°C) = 455 - 90*δ_{H2O}, where δ_{H2O} denotes the chemical shift of the supernatant water signal[43]. 2D hNH spectra were recorded on all samples while 2D hCH spectra were recorded on UL-HDAg$^{1\text{-}60}$, EL-HDAg$^{1\text{-}60}$ and GRK-HDAg$^{1\text{-}60}$ samples. 3D hCANH, hNCAH, hCONH, hNcoCAH (with reverse MIRROR transfer[44], Fig. S11) and hCAcoNH were recorded on the UL-HDAg$^{1\text{-}60}$ sample for backbone proton and heteronuclei assignments. 3D hCCH-TOBSY experiments[28] were recorded on the UL-HDAg$^{1\text{-}60}$ and GRK-HDAg$^{1\text{-}60}$ samples for side chain proton and carbon assignments. To complete the assignment, 3D hCONH, hCAcoNH, were recorded on the EL-HDAg$^{1\text{-}60}$ and GRK-HDAg$^{1\text{-}60}$ samples.

Bulk proton longitudinal relaxation times $T_1(^1H)$ were determined using a saturation recovery sequence with 16 variable delays up to 8 s. Bulk proton transverse relaxation times $T_2'(^1H)$ were determined using a Hahn-echo sequence with 14 and 12 variable echo delays up to 3.5 and 5 ms at 850 and 1.2 GHz respectively. Further details of the acquisition parameters are given in the Supplementary Tables S7-11.

All spectroscopic data were processed using Topspin 4.0.8 (Bruker Biospin) with zero filling to the double amount of data points and a shifted sine-bell apodization function in the direct and indirect dimensions with SSB= 2.5. Acquisition in the direct dimension was cut to 12.9 ms. The spectra were analyzed using CcpNmr Analysis 2.5[45,46].

Relaxation analysis

Bulk relaxation times were extracted from a series of 1D hcH and hnH experiments using the relaxation analysis tool in Topspin 4.0.8 (Bruker Biospin). Bulk homogeneous line widths $\Delta^{\mathrm{homo}}(^1H)$ have been determined using the relationship $\Delta^{\mathrm{homo}}(^1H) = 1/\pi T_2'$. The site-specific total linewidths were extracted from the CP-based 2D hCH and 2D hNH spectra using the Gaussian function in CcpNmr Analysis 2.5[45,46].

Data Analysis

The chemical shift differences between DUL-S-HDAg and DUL-HDAg$^{1\text{-}60}$ were calculated for isolated resonances in the 2D hNH spectra for the H_N and N nuclei, respectively, using the following equations: $\Delta\delta_{HN} = |\Delta\delta_{HN[S]} - \Delta\delta_{HN[S\ 1\text{-}60]}|$ and $\Delta\delta_N = |\Delta\delta_{N[S]} - \Delta\delta_{N[S\ 1\text{-}60]}|$. The same equations were used to calculate the chemical shift differences between UL-HDAg$^{1\text{-}60}$ and UL-HDAg$^{1\text{-}60}$ without tag. Threshold values were set at one standard deviation (σ) above the mean chemical shift difference.

Secondary structure elements were predicted from the secondary chemical shifts using the following equation: $\Delta\delta C_\alpha - \Delta\delta C_\beta = (\delta C_\alpha - \delta C_{\alpha\,rc}) - (\delta C_\beta - \delta C_{\beta\,rc})$ as described in Wang et al.[35] and where rc represents random coil[47].

Assignment deposition

^{1}H, ^{13}C and ^{15}N backbone and side chain chemical shifts of UL-HDAg$^{1\text{-}60}$ have been deposited in the Biological Magnetic Resonance Data Bank (BMRB) (http://www.bmrb.wisc.edu) under accession number 52512.

Acknowledgments

Financial support from the ANRS (ECTZ158948, ECTZ205074, ECTZ205154), the China Scholarship Council (202008620095) and the Schweizerischer Nationalfonds zur Förderung der Wissenschaftlichen Forschung (SNF grant no. 200021_201070/1) is gratefully acknowledged. The authors acknowledge Andreas Hunkeler for the rotor filling tools. They also thank Stephan Urban for cloning the S-HDAg sequence into the pEU-E01-MCS vector. The Böckmann laboratory is very grateful to Jérôme Vansuyt of the company Florimond-Desprez for kindly providing non treated durum wheat seeds for the preparation of WG extracts.

Supporting information

The supporting information is available, containing additional spectra, analysis and detailed NMR parameters for all experiments recorded.

References

(1) Negro, F. Hepatitis D Virus Coinfection and Superinfection. *Cold Spring Harb. Perspect. Med.* **2014**, *4* (11), a021550. https://doi.org/10.1101/cshperspect.a021550.

(2) Lorenc, B.; Sikorska, K.; Stalke, P.; Bielawski, K.; Ziętkowski, D. Hepatitis D, B and C Virus (HDV/HBV/HCV) Coinfection as a Diagnostic Problem and Therapeutic Challenge. *Clin. Exp. Hepatol.* **2017**, *3* (1), 23–27. https://doi.org/10.5114/ceh.2017.65500.

(3) Kos, A.; Dijkema, R.; Arnberg, A. C.; van der Meide, P. H.; Schellekens, H. The Hepatitis Delta (Delta) Virus Possesses a Circular RNA. *Nature* **1986**, *323* (6088), 558–560. https://doi.org/10.1038/323558a0.

(4) Kuo, M. Y.; Sharmeen, L.; Dinter-Gottlieb, G.; Taylor, J. Characterization of Self-Cleaving RNA Sequences on the Genome and Antigenome of Human Hepatitis Delta Virus. *J Virol* **1988**, *62* (12), 4439–4444. https://doi.org/10.1128/JVI.62.12.4439-4444.1988.

(5) Kuo, M. Y.; Chao, M.; Taylor, J. Initiation of Replication of the Human Hepatitis Delta Virus Genome from Cloned DNA: Role of Delta Antigen. *J Virol* **1989**, *63* (5), 1945–1950. https://doi.org/10.1128/jvi.63.5.1945-1950.1989.

(6) Abbas, Z. Life Cycle and Pathogenesis of Hepatitis D Virus: A Review. *World J. Hepatol.* **2013**, *5* (12), 666–675. https://doi.org/10.4254/wjh.v5.i12.666.

(7) O'Malley, B.; Lazinski, D. W. Roles of Carboxyl-Terminal and Farnesylated Residues in the Functions of the Large Hepatitis Delta Antigen. *J. Virol.* **2005**, *79* (2), 1142–1153. https://doi.org/10.1128/JVI.79.2.1142-1153.2005.

(8) Chiou, W.-C.; Lu, H.-F.; Chen, J.-C.; Lai, Y.-H.; Chang, M.-F.; Huang, Y.-L.; Tien, N.; Huang, C. Identification of a Novel Interaction Site between the Large Hepatitis Delta Antigen and Clathrin That Regulates the Assembly of Genotype III Hepatitis Delta Virus. *Virol. J.* **2022**, *19* (1), 163. https://doi.org/10.1186/s12985-022-01866-3.

(9) Bell, P.; Brazas, R.; Ganem, D.; Maul, G. G. Hepatitis Delta Virus Replication Generates Complexes of Large Hepatitis Delta Antigen and Antigenomic RNA That Affiliate with and Alter Nuclear Domain 10. *J. Virol.* **2000**, *74* (11), 5329–5336. https://doi.org/10.1128/JVI.74.11.5329-5336.2000.

(10) Zi, J.; Gao, X.; Du, J.; Xu, H.; Niu, J.; Chi, X. Multiple Regions Drive Hepatitis Delta Virus Proliferation and Are Therapeutic Targets. *Front. Microbiol.* **2022**, *13*, 838382. https://doi.org/10.3389/fmicb.2022.838382.

(11) Zuccola, H.; Rozzelle, J.; Lemon, S.; Erickson, B.; Hogle, J. Structural Basis of the Oligomerization of Hepatitis Delta Antigen. *Structure* **1998**, *6* (7), 821–830.

(12) Cornillez-Ty, C. T.; Lazinski, D. W. Determination of the Multimerization State of the Hepatitis Delta Virus Antigens In Vivo. *J. Virol.* **2003**, *77* (19), 10314–10326. https://doi.org/10.1128/JVI.77.19.10314-10326.2003.

(13) Poisson, F.; Baillou, F.; Dubois, F.; Janvier, B.; Roingeard, P.; Goudeau, A. Immune Response to Synthetic Peptides of Hepatitis Delta Antigen. *J. Clin. Microbiol.* **1993**, *31* (9), 2343–2349. https://doi.org/10.1128/jcm.31.9.2343-2349.1993.

(14) Poisson, F.; Roingeard, P.; Goudeau, A. Direct Investigation of Protein RNA-Binding Domains Using Digoxigenin-Labelled RNAs and Synthetic Peptides: Application to the Hepatitis Delta Antigen. *J. Virol. Methods* **1995**, *55* (3), 381–389. https://doi.org/10.1016/0166-0934(95)00087-5.

(15) Wang, J. G.; Lemon, S. M. Hepatitis Delta Virus Antigen Forms Dimers and Multimeric Complexes in Vivo. *J. Virol.* **1993**, *67* (1), 446–454. https://doi.org/10.1128/jvi.67.1.446-454.1993.

(16) Alves, C.; Cheng, H.; Tavanez, J. P.; Casaca, A.; Gudima, S.; Roder, H.; Cunha, C. Structural and Nucleic Acid Binding Properties of Hepatitis Delta Virus Small Antigen. *World J. Virol.* **2017**, *6* (2), 26–35. https://doi.org/10.5501/wjv.v6.i2.26.

(17) Defenbaugh, D. A.; Johnson, M.; Chen, R.; Zheng, Y. Y.; Casey, J. L. Hepatitis Delta Antigen Requires a Minimum Length of the Hepatitis Delta Virus Unbranched Rod RNA Structure for Binding. *J. Virol.* **2009**, *83* (9), 4548–4556. https://doi.org/10.1128/JVI.02467-08.

(18) Takai, K.; Sawasaki, T.; Endo, Y. Practical Cell-Free Protein Synthesis System Using Purified Wheat Embryos. *Nat. Protoc.* **2010**, *5* (2), 227–238. https://doi.org/10.1038/nprot.2009.207.

(19) Fogeron, M.-L.; Lecoq, L.; Cole, L.; Harbers, M.; Böckmann, A. Easy Synthesis of Complex Biomolecular Assemblies: Wheat Germ Cell-Free Protein Expression in Structural Biology. *Front. Mol. Biosci.* **2021**, *8*, 639587. https://doi.org/10.3389/fmolb.2021.639587.

(20) Jirasko, V.; Lakomek, N.; Penzel, S.; Fogeron, M.; Bartenschlager, R.; Meier, B. H.; Böckmann, A. Proton-Detected Solid-State NMR of the Cell-Free Synthesized α-Helical Transmembrane Protein NS4B from Hepatitis C Virus. *ChemBioChem* **2020**, *21* (10), 1453–1460. https://doi.org/10.1002/cbic.201900765.

(21) Jirasko, V.; Lends, A.; Lakomek, N.; Fogeron, M.; Weber, M. E.; Malär, A. A.; Penzel, S.; Bartenschlager, R.; Meier, B. H.; Böckmann, A. Dimer Organization of Membrane-Associated NS5A of Hepatitis C Virus as Determined by Highly Sensitive ^{1}H-Detected Solid-State NMR. *Angew. Chem. Int. Ed.* **2021**, *60* (10), 5339–5347. https://doi.org/10.1002/anie.202013296.

(22) Brigandat, L.; Laux, M.; Marteau, C.; Cole, L.; Böckmann, A.; Lecoq, L.; Fogeron, M.-L.; Callon, M. NMR Side-Chain Assignments of the Crimean–Congo Hemorrhagic Fever Virus Glycoprotein n Cytosolic Domain. *Magn. Reson.* **2024**, *5* (2), 95–101. https://doi.org/10.5194/mr-5-95-2024.

(23) Le Marchand, T.; Schubeis, T.; Bonaccorsi, M.; Paluch, P.; Lalli, D.; Pell, A. J.; Andreas, L. B.; Jaudzems, K.; Stanek, J.; Pintacuda, G. 1H-Detected Biomolecular NMR under Fast Magic-Angle Spinning. *Chem. Rev.* **2022**, *122* (10), 9943–10018. https://doi.org/10.1021/acs.chemrev.1c00918.

(24) Nishiyama, Y.; Hou, G.; Agarwal, V.; Su, Y.; Ramamoorthy, A. Ultrafast Magic Angle Spinning Solid-State NMR Spectroscopy: Advances in Methodology and Applications. *Chem. Rev.* **2023**, *123* (3), 918–988. https://doi.org/10.1021/acs.chemrev.2c00197.

(25) Lecoq, L.; Schledorn, M.; Wang, S.; Smith-Penzel, S.; Malär, A. A.; Callon, M.; Nassal, M.; Meier, B. H.; Böckmann, A. 100 kHz MAS Proton-Detected NMR Spectroscopy of

Hepatitis b Virus Capsids. *Front. Mol. Biosci.* **2019**, *6*, 58. https://doi.org/10.3389/fmolb.2019.00058.

(26)Gardiennet, C.; Schütz, A. K.; Hunkeler, A.; Kunert, B.; Terradot, L.; Böckmann, A.; Meier, B. H. A Sedimented Sample of a 59 kDa Dodecameric Helicase Yields High-Resolution Solid-State NMR Spectra. *Angew. Chem. Int. Ed Engl.* **2012**, *51* (31), 7855–7858. https://doi.org/10.1002/anie.201200779.

(27) Callon, M.; Malär, A. A.; Pfister, S.; Římal, V.; Weber, M. E.; Wiegand, T.; Zehnder, J.; Chávez, M.; Cadalbert, R.; Deb, R.; Däpp, A.; Fogeron, M.-L.; Hunkeler, A.; Lecoq, L.; Torosyan, A.; Zyla, D.; Glockshuber, R.; Jonas, S.; Nassal, M.; Ernst, M.; Böckmann, A.; Meier, B. H. Biomolecular Solid-State NMR Spectroscopy at 1200 MHz: The Gain in Resolution. *J. Biomol. NMR* **2021**, *75* (6–7), 255–272. https://doi.org/10.1007/s10858-021-00373-x.

(28) Stanek, J.; Andreas, L. B.; Jaudzems, K.; Cala, D.; Lalli, D.; Bertarello, A.; Schubeis, T.; Akopjana, I.; Kotelovica, S.; Tars, K.; Pica, A.; Leone, S.; Picone, D.; Xu, Z.-Q.; Dixon, N. E.; Martinez, D.; Berbon, M.; El Mammeri, N.; Noubhani, A.; Saupe, S.; Habenstein, B.; Loquet, A.; Pintacuda, G. NMR Spectroscopic Assignment of Backbone and Side-Chain Protons in Fully Protonated Proteins: Microcrystals, Sedimented Assemblies, and Amyloid Fibrils. *Angew. Chem. Int. Ed.* **2016**, *55* (50), 15504–15509. https://doi.org/10.1002/anie.201607084.

(29) Tonelli, M.; Singarapu, K. K.; Makino, S.; Sahu, S. C.; Matsubara, Y.; Endo, Y.; Kainosho, M.; Markley, J. L. Hydrogen Exchange during Cell-Free Incorporation of Deuterated Amino Acids and an Approach to Its Inhibition. *J. Biomol. NMR* **2011**, *51* (4), 467–476. https://doi.org/10.1007/s10858-011-9575-4.

(30) Tan, K. O.; Agarwal, V.; Lakomek, N.-A.; Penzel, S.; Meier, B. H.; Ernst, M. Efficient Low-Power TOBSY Sequences for Fast MAS. *Solid State NMR* **2018**, *89*, 27–34. https://doi.org/10.1016/j.ssnmr.2017.11.003.

(31) Maslennikov, I.; Klammt, C.; Hwang, E.; Kefala, G.; Okamura, M.; Esquivies, L.; Mörs, K.; Glaubitz, C.; Kwiatkowski, W.; Jeon, Y. H.; Choe, S. Membrane Domain Structures of Three Classes of Histidine Kinase Receptors by Cell-Free Expression and Rapid NMR Analysis. *Proc. Natl. Acad. Sci.* **2010**, *107* (24), 10902–10907. https://doi.org/10.1073/pnas.1001656107.

(32) Hoffmann, B.; Löhr, F.; Laguerre, A.; Bernhard, F.; Dötsch, V. Protein Labeling Strategies for Liquid-State NMR Spectroscopy Using Cell-Free Synthesis. *Prog. Nucl. Magn. Reson. Spectrosc.* **2018**, *105*, 1–22. https://doi.org/10.1016/j.pnmrs.2017.11.004.

(33) Dubey, A.; Kadumuri, R. V.; Jaipuria, G.; Vadrevu, R.; Atreya, H. S. Rapid NMR Assignments of Proteins by Using Optimized Combinatorial Selective Unlabeling. *ChemBioChem* **2016**, *17* (4), 334–340. https://doi.org/10.1002/cbic.201500513.

(34) Hein, C.; Löhr, F.; Schwarz, D.; Dötsch, V. Acceleration of Protein Backbone NMR Assignment by Combinatorial Labeling: Application to a Small Molecule Binding Study. *Biopolymers* **2017**, *107* (5). https://doi.org/10.1002/bip.23013.

(35) Wang, Y.; Jardetzky, O. Probability-based Protein Secondary Structure Identification Using Combined NMR Chemical-shift Data. *Protein Sci.* **2002**, *11* (4), 852–861. https://doi.org/10.1110/ps.3180102.

(36) Wishart, D. S.; Bigam, C. G.; Holm, A.; Hodges, R. S.; Sykes, B. D. 1H, 13C and 15N Random Coil NMR Chemical Shifts of the Common Amino Acids. I. Investigations of Nearest-Neighbor Effects. *J Biomol NMR* **1995**, *5* (1), 67–81. https://doi.org/10.1007/BF00227471.

(37) Wang, S.; Fogeron, M.-L.; Schledorn, M.; Dujardin, M.; Penzel, S.; Burdette, D.; Berke, J. M.; Nassal, M.; Lecoq, L.; Meier, B. H.; Böckmann, A. Combining Cell-Free Protein Synthesis and NMR Into a Tool to Study Capsid Assembly Modulation. *Front. Mol. Biosci.* **2019**, *6*, 67. https://doi.org/10.3389/fmolb.2019.00067.

(38) Smith, A. A.; Ravotti, F.; Testori, E.; Cadalbert, R.; Ernst, M.; Böckmann, A.; Meier, B. H. Partially-Deuterated Samples of HET-s(218–289) Fibrils: Assignment and Deuterium Isotope Effect. *J. Biomol. NMR* **2017**. https://doi.org/10.1007/s10858-016-0087-0.

(39) Lin, B. C.; Defenbaugh, D. A.; Casey, J. L. Multimerization of Hepatitis Delta Antigen Is a Critical Determinant of RNA Binding Specificity. *J. Virol.* **2010**, *84* (3), 1406–1413. https://doi.org/10.1128/JVI.01723-09.

(40) Griffin, B. L.; Chasovskikh, S.; Dritschilo, A.; Casey, J. L. Hepatitis Delta Antigen Requires a Flexible Quasi-Double-Stranded RNA Structure To Bind and Condense Hepatitis Delta Virus RNA in a Ribonucleoprotein Complex. *J. Virol.* **2014**, *88* (13), 7402–7411. https://doi.org/10.1128/JVI.00443-14.

(41) Abeywickrama-Samarakoon, N.; Cortay, J.-C.; Sureau, C.; Müller, S.; Alfaiate, D.; Guerrieri, F.; Chaikuad, A.; Schröder, M.; Merle, P.; Levrero, M.; Dény, P. Hepatitis Delta Virus Histone Mimicry Drives the Recruitment of Chromatin Remodelers for Viral RNA Replication. *Nat. Commun.* **2020**, *11* (1), 419. https://doi.org/10.1038/s41467-020-14299-9.

(42) Fogeron, M.-L.; Badillo, A.; Penin, F.; Böckmann, A. Wheat Germ Cell-Free Overexpression for the Production of Membrane Proteins. In *Membrane Protein Structure and Function Characterization*; Lacapere, J.-J., Ed.; Springer New York: New York, NY, 2017; Vol. 1635, pp 91–108. https://doi.org/10.1007/978-1-4939-7151-0_5.

(43) Böckmann, A.; Gardiennet, C.; Verel, R.; Hunkeler, A.; Loquet, A.; Pintacuda, G.; Emsley, L.; Meier, B. H.; Lesage, A. Characterization of Different Water Pools in Solid-State NMR Protein Samples. *J. Biomol. NMR* **2009**, *45* (3), 319–327. https://doi.org/10.1007/s10858-009-9374-3.

(44) Wittmann, J. J.; Agarwal, V.; Hellwagner, J.; Lends, A.; Cadalbert, R.; Meier, B. H.; Ernst, M. Accelerating Proton Spin Diffusion in Perdeuterated Proteins at 100 kHz MAS. *J. Biomol. NMR* **2016**, *66* (4), 233–242. https://doi.org/10.1007/s10858-016-0071-8.

(45) Vranken, W. F.; Boucher, W.; Stevens, T. J.; Fogh, R. H.; Pajon, A.; Llinas, M.; Ulrich, E. L.; Markley, J. L.; Ionides, J.; Laue, E. D. The CCPN Data Model for NMR Spectroscopy: Development of a Software Pipeline. *Proteins Struct. Funct. Bioinforma.* **2005**, *59* (4), 687–696. https://doi.org/10.1002/prot.20449.

(46) Stevens, T. J.; Fogh, R. H.; Boucher, W.; Higman, V. A.; Eisenmenger, F.; Bardiaux, B.; Van Rossum, B. J.; Oschkinat, H.; Laue, E. D. A Software Framework for Analysing Solid-State MAS NMR Data. *J Biomol NMR* **2011**, *51* (4), 437–447. https://doi.org/10.1007/s10858-011-9569-2.

(47) Wishart, D. S.; Sykes, B. D. The 13C Chemical-Shift Index: A Simple Method for the Identification of Protein Secondary Structure Using 13C Chemical-Shift Data. *J. Biomol. NMR* **1994**, *4* (2), 171–180. https://doi.org/10.1007/BF00175245.

For Table of Contents Only: